Plane-wave migration in tilted coordinates

Guojian Shan and Biondo Biondi

ABSTRACT

Most existing one-way wave-equation migration algorithms have difficulty in imaging steep dips in a medium with strong lateral velocity variation. We propose a new one-way wave-equation-based migration, called "plane-wave migration in tilted coordinates." The surface data are converted to plane-wave source data by slant-stacking processing, and each resulting plane-wave source dataset is migrated independently in a tilted coordinate system with an extrapolation direction determined by the source plane-wave direction at the surface. For most waves illuminating steeply dipping reflectors, the extrapolation direction is closer to their propagation direction in the tilted coordinates. Therefore, plane-wave migration in tilted coordinates can correctly image steeply dipping reflectors, even by applying one-way extrapolators. In a well-chosen tilted coordinate system, waves that overturn in conventional vertical Cartesian coordinates do not overturn in the new coordinate system. Using plane-wave migration in tilted coordinates, we can image overturned energy with much lower cost compared to reverse-time migration.

INTRODUCTION

Kirchhoff migration has been widely applied in seismic processing due to its relatively low cost and flexibility. However, it cannot provide reliable images where multipathing occurs. Wave-equation migration, which is performed by recursive wavefield extrapolation, has been demonstrated to overcome these limitations and produce better images in areas of complex geology.

It is well known that in a single-shot experiment waves propagate upward and downward simultaneously. Reverse-time migration (Whitmore, 1983; Baysal et al., 1983; Biondi and Shan, 2002), which solves the full wave equation directly and mimics wave propagation naturally, is expensive for routine use in today's computing facilities. As a consequence, downward continuation migration Claerbout (1985), which are based on one-way wave-equation wavefield extrapolation and are much cheaper than reverse-time migration, are widely used in the industry.

Conventional downward-continuation methods extrapolate wavefields using the one-way wave equation in vertical Cartesian coordinates. For a medium without lateral velocity variation, the phase-shift method (Gazdag, 1978) can be applied, and the one-way wave-equation can model waves propagating in a direction up to 90° away

from the extrapolation direction. But in a laterally varying medium, it is very difficult to model waves propagating in a direction far from the extrapolation direction using a one-way wavefield extrapolator. Many methods have been developed to improve the accuracy of the one-way wavefield extrapolator in laterally varying media, such as Fourier finite-difference (Ristow and Ruhl, 1994; Biondi, 2002), the general screen propagator (de Hoop, 1996; Huang and Wu, 1996) and optimized finite difference (Lee and Suh, 1985) with a phase correction (Li, 1991). Even if we could model waves accurately up to 90° using the one-way wavefield extrapolator in laterally varying media, overturned waves, which travel downward first and then curve upward, are filtered away during the wavefield extrapolation because of the assumption that the waves propagate vertically only in one direction: downward for source wavefields and upward for receiver wavefields. However, overturned waves and waves propagating at high angles play a key role in imaging steeply dipping reflectors, such as salt flank and faults. As a consequence, imaging these steeply dipping reflectors remains a major problem in downward continuation migration.

Work has been done to image the steeply dipping reflectors with one-way wavefield extrapolators by coordinate transformation. This includes tilted coordinates (Higginbotham et al., 1985; Etgen, 2002), the combination of downward continuation and horizontal continuation (Zhang and McMechan, 1997), or wavefield extrapolation in general coordinates, such as ray coordinates (Nichols, 1994) and Riemannian coordinates (Sava and Fomel, 2005; Shragge, 2006).

In tilted coordinates, waves traveling along the extrapolation direction are most accurately modeled, and the maximum angle of their propagation direction from the extrapolation direction that can be handled is determined by the accuracy of the wavefield extrapolator. For a point source, where waves travel in all directions from a point, it is impossible for one tilted coordinate system to cover all these directions. But for a plane-wave source, waves travel in a similar direction from all spacial points at the surface, and thus most of them can be modeled accurately in a tilted coordinate system with a well-chosen tilting direction. In this paper, we apply plane-wave migration (Whitmore, 1995; Rietveld, 1995; Duquet et al., 2001; Liu et al., 2002; Zhang et al., 2005) in tilted coordinates. Plane-wave migration has been demonstrated to be a useful tool in seismic imaging. By slant-stacking, the recorded surface data are synthesized into areal plane-wave-source gathers, which are what would be recorded if plane-wave sources were excited at the surface. A plane-wave source is characterized by a ray parameter, and its take-off angle can be calculated from the ray parameter, given the velocity at the surface. Each areal plane-source gather is migrated independently, similar to shot-profile migration, and the image is formed by stacking the images of all possible plane-wave sources. Given a plane-wave source, we tilt the coordinate system according to its take-off angle. For most waves, the resulting extrapolation direction is closer to the propagation direction, and thus we can image steeply dipping reflectors correctly using one-way wavefield extrapolators. Plane-wave migration is potentially more efficient than shot-profile migration (Zhang et al., 2005; Etgen, 2005). To image steeply dipping reflectors or overturned waves, a large migration aperture is required to cover the whole propagation path of source and receiver

waves. In shot-profile migration, this requires large padding in space. In contrast, plane-wave migration uses the whole seismic survey as the migration aperture. It is well known that one-way wave-equation shot-profile migration is much cheaper than reverse-time migration. Compared to conventional plane-wave migration, the cost of plane-wave migration in tilted coordinates is a little higher because of the data and velocity model interpolation, but it is still much lower than reverse-time migration.

This paper is organized as follows: we begin with a brief review of one-way wave-equation migration and plane-wave migration. Then we introduce how to extrapolate the wavefield in a tilted coordinate system and describe plane-wave migration in tilted coordinates. Finally, we demonstrate our technique with synthetic data examples.

ONE-WAY WAVE EQUATION MIGRATION

Surface seismic data are usually recorded as shot gathers. Each shot gather represents a point-source exploding experiment. The most straightforward way to obtain the subsurface image of the earth is shot-profile migration, in which we obtain the local image of each experiment by migrating each shot gather independently and form the whole image of the subsurface by stacking all the local images. Migrating one shot gather using a typical shot-profile migration algorithm includes two steps. First, source and receiver wavefields are extrapolated from the surface to all depths in the subsurface. Second, the images are constructed by cross-correlating the source and receiver wavefields.

The propagation of waves in the subsurface is approximately governed by a two-way acoustic wave equation. In an isotropic medium, it is defined as follows:

$$\frac{1}{v^2}\frac{\partial^2}{\partial t^2}P = \left(\frac{\partial^2}{\partial x^2} + \frac{\partial^2}{\partial z^2}\right)P, \tag{1}$$

where $P = P(x, z, t)$ is the pressure field and $v = v(x, z)$ is the velocity of the medium. To reduce computational costs, we usually use the one-way instead of two-way wave equations for wavefield extrapolation:

$$\frac{\partial}{\partial z}S = -\frac{i\omega}{v}\sqrt{1 + \left(\frac{v}{\omega}\frac{\partial}{\partial x}\right)^2}\,S, \tag{2}$$

$$\frac{\partial}{\partial z}R = +\frac{i\omega}{v}\sqrt{1 + \left(\frac{v}{\omega}\frac{\partial}{\partial x}\right)^2}\,R, \tag{3}$$

for wavefield extrapolation, where ω is angular frequency, $S = S(s_x, x, z, \omega)$ is the source wavefield, $R = R(s_x, x, z, \omega)$ is the receiver wavefield, and s_x is the source location. Given the propagation direction of the source and receiver wavefields, we use the down-going one-way wave equation (equation 2) for the source wavefield and the up-going one-way wave equation (equation 3) for the receiver wavefield. Both are obtained by splitting the two-way acoustic equation (Zhang, 1993). After the

wavefield extrapolation, we have the source and receiver wavefields at all depths and the image is constructed by cross-correlating the source and receiver wavefields as follows:

$$I_{s_x} = \int S^*(s_x, x, z, \omega) R(s_x, x, z, \omega) d\omega, \tag{4}$$

where S^* is the complex conjugate of the source wavefield S. Finally the whole image is generated by stacking the images of all the shots as follows:

$$I = \int I_{s_x} ds_x. \tag{5}$$

If there is no lateral velocity variation, equations 2 and 3 can be solved by the phase-shift method in the frequency-wavenumber domain with accuracy up to 90°. Otherwise, an approximation for the square root operator has to be made to solve equations 2 and 3 numerically. The accuracy of a wavefield extrapolator determines the maximum angle between the propagation direction and the vertical direction that can be modeled accurately. most algorithms can model waves that propagate almost vertically downward. For example, the classic 15° equation (Claerbout, 1971) can handle waves propagating 15° from the vertical direction. However, most algorithms cannot model waves propagating almost horizontally in a medium with strong lateral variation. Finite-difference methods handle lateral variation of the media well, but the cost of improving the accuracy at high angles is high. Hybrid algorithms such as Fourier finite-difference take advantage of both the finite-difference and phase-shift methods. When the lateral variation of the medium is mild, phase-shift plays the important role and can achieve good accuracy. The finite-difference part becomes more important where the actual velocity value is far from the reference velocity, but again is difficult to propagate high-angle energy accurately with a reasonable cost. It is difficult to solve the one-way wave equation accurately to model high-angle energy in a medium with strong lateral variation.

One-way wave equations also function as dip filters. During the source wavefield extrapolation, only the down-going energy is permitted using the down-going one-way wave equation; up-going energy is filtered out. Similarly, the down-going energy is filtered out during the receiver wavefield extrapolation. Therefore, overturned energy is filtered out in both source and receiver wavefields in conventional downward continuation migration.

Conventional downward continuation migration is not sufficient for imaging steeply dipping reflectors, since they are mainly illuminated by high-angle and overturned energy. These are the two main migration issues that we attempt to resolve with plane-wave migration in tilted coordinates.

PLANE-WAVE SOURCE MIGRATION

Shot gathers can also be synthesized into a new dataset to represent a physical experiment that is not performed in reality. One of the most important examples is to

synthesize shot gathers into plane-wave source gathers. A plane-wave source gather represents what would be recorded if a planar source were excited at the surface with geophones covering the whole area. It can also be regarded as the accurate phase-encoding of the shot gathers (Liu et al., 2002). Plane-wave source gathers can be generated by slant-stacking receiver gathers. The process can be described as follows:

$$R_p(p_x, r_x, z=0, \omega) = \int R(s_x, r_x, z=0, \omega) e^{i\omega s_x p_x} ds_x, \tag{6}$$

where p_x is the ray parameter for the x-axis, s_x is the source location, and r_x is the receiver location at the surface. Its corresponding plane-wave source wavefield at the surface is

$$S_p(p_x, r_x, z=0, \omega) = e^{i\omega r_x p_x}. \tag{7}$$

As with the Fourier transformation, we can transform the plane-wave source gathers back to shot gathers by inverse slant-stacking (Claerbout, 1985) as follows:

$$R(s_x, r_x, z=0, \omega) = \int \omega R_p(p_x, r_x, z=0, \omega) e^{-i\omega s_x p_x} dp_x. \tag{8}$$

In contrast to the inverse Fourier transformation, the kernel of the integral is weighted by the angular frequency ω. This inverse transformation weighting function is also called ρ filter in Radon-transform literature.

As with shot-profile migration, there are two steps to migrate a plane-wave source gather by a typical plane-wave migration method. First, the source wavefield S_p and receiver wavefield R_p are extrapolated into all depths in the subsurface independently, using the one-way wave equations 2 and 3, respectively. Second, the image of a plane-wave source with a ray parameter p_x is constructed by cross-correlating the source and receiver wavefields weighted with the angular frequency ω:

$$I_{p_x}(x, z) = \int \omega {S_p}^*(p_x, x, z, \omega) R_p(p_x, x, z, \omega) d\omega, \tag{9}$$

where ${S_p}^*$ is the conjugate complex of the source wavefield S_p. The whole image is formed by stacking the images of all possible plane-wave sources:

$$I_p = \int\int I_{p_x}(x, z) dp_x. \tag{10}$$

Because both slant-stacking and migration are linear operators, the image of the plane-wave migration I_p is equivalent to the image obtained by shot-profile migration (Liu et al., 2002; Zhang et al., 2005). In the discrete form, in practice we need a sufficient number of p_x to make the two images equivalent.

WAVEFIELD EXTRAPOLATION IN TILTED COORDINATES

The extrapolation direction plays a key role in one-way wave-equation wavefield extrapolation, since the waves traveling along the extrapolation direction are modeled

the most accurately. However, the extrapolation direction has no physical meaning and it is only a direction artificially assigned in numerical algorithms. In conventional downward continuation migration, we use vertical Cartesian coordinates and extrapolate wavefields vertically. The extrapolation direction can be changed by rotating the coordinates. It is well known that the acoustic equation (equation 1) is invariant to coordinate rotations as follows:

$$\begin{pmatrix} x' \\ z' \end{pmatrix} = \begin{pmatrix} \cos\theta & \sin\theta \\ -\sin\theta & \cos\theta \end{pmatrix} \begin{pmatrix} x \\ z \end{pmatrix}. \tag{11}$$

We call the new coordinate system (x', z') a tilted Cartesian coordinate system (or tilted coordinate system) and the angle θ the tilting angle for the coordinate system.

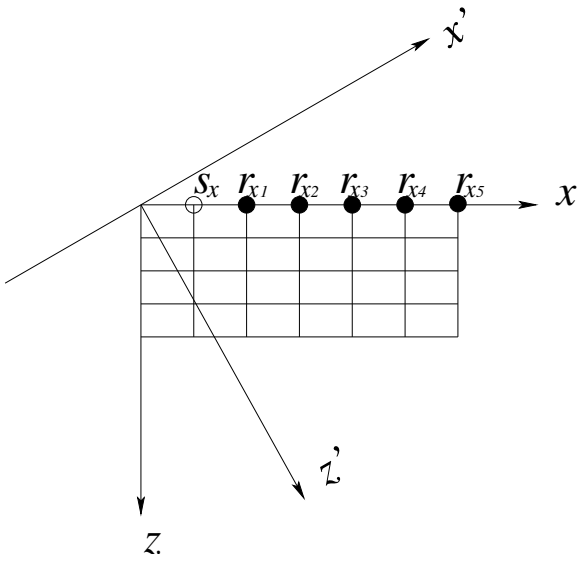

Figure 1: Coordinate system rotation: (x, z) are conventional vertical Cartesian coordinates, (x', z') are tilted coordinates, s_x represents the source location, and $r_{xi}, i = 1, 2, \cdots, 5$ represent receiver locations. The source and receivers are on regular grids in vertical Cartesian coordinates.

As in the vertical Cartesian coordinates, the up-going and down-going one-way wave equations can be obtained by splitting the acoustic wave equation in the tilted coordinate system (x', z'):

$$\frac{\partial}{\partial z'} S = -\frac{i\omega}{v} \sqrt{1 + \left(\frac{v}{\omega} \frac{\partial}{\partial x'} \right)^2} S, \tag{12}$$

$$\frac{\partial}{\partial z'} R = +\frac{i\omega}{v} \sqrt{1 + \left(\frac{v}{\omega} \frac{\partial}{\partial x'} \right)^2} R. \tag{13}$$

The extrapolation direction of equations 12 and 13 parallels the z' axis, which is θ from the vertical direction. Figure 1 illustrates the coordinate transformation, where (x, z) are vertical Cartesian coordinates and (x', z') are tilted coordinates, s_x represents the source location and $r_{x_1}, r_{x_2}, \cdots, r_{x_5}$ represent the corresponding receiver locations. The accuracy of the one-way wavefield extrapolators is still very important for wavefield extrapolation in tilted coordinates. The more accurately we design the wavefield extrapolator, the less sensitive the migration is to the coordinates. With an extrapolator that is not very accurate, such as the 15° equation, waves well handled in

one coordinate system are not handled in one that is slightly rotated. In contrast, with an accurate extrapolator, waves can be handled in both tilted coordinate systems. Since one-way wave equations in tilted coordinates are exactly the same as those in vertical Cartesian coordinates, all the methods used to improve the accuracy in the conventional Cartesian coordinates still work in tilted coordinates.

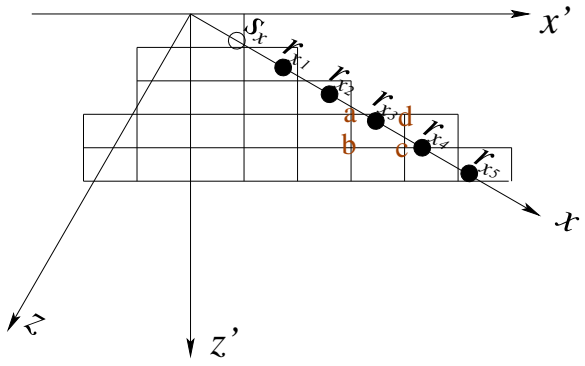

Figure 2: Source and receivers in grids of a tilted coordinate system: (x, z) are conventional vertical Cartesian coordinates, (x', z') are tilted coordinates, s_x represents the source location, and $r_{xi}, i = 1, 2, \cdots, 5$ represent receiver locations. Neither source nor receiver locations are on regular grids in the tilted coordinate system. Their wavefield values must be interpolated onto regular grids around the slanted line in tilted coordinates. The wavefield on r_{x3} is interpolated onto the grids a, b, c, and d.

To extrapolate wavefields in a tilted coordinate system, it is necessary to interpolate the surface dataset, velocity model and image between the coordinate systems and migrate the dataset on a slanted line in implementation. In Figure 1, the source and receivers are on regular grids in conventional Cartesian coordinates. Figure 2 shows the source and receivers in meshes in the tilted coordinates (x', z'). Source and receivers are on an inclined line defined by the equation

$$x' \cos\theta - z' \sin\theta = 0. \tag{14}$$

They are not on regular grids in tilted coordinates. To run wavefield extrapolation, the dataset received at the surface has to be interpolated onto the regularized grids around the inclined line in the new coordinate system (x', z'). For instance, the value of the wavefield at r_{x_3} has to be interpolated onto the grids a,b,c and d in Figure 2. The velocity must also be interpolated onto the grids in the coordinates (x', z'). In tilted coordinates, the survey is taken on a long, slanted line defined by equation 14. We extrapolate the wavefield with the surface dataset on the slanted line injected at each depth step. We begin the wavefield extrapolation at the point $z' = 0$. For the i-th step extrapolation, when the depth level $z' = i\Delta z$ intersects the slanted line, we add the measured wavefield on the slanted line to the wavefield extrapolated from its previous depth level. After we inject the wavefields on the slanted line, the wavefield extrapolation is the same as the conventional one.

Figure 3 shows a velocity model revised from the Sigsbee 2A model (Sava, 2006). The sediment part of the model is extended vertically and horizontally to receive the

overturned waves from the overhanging salt flank at the surface. The rays correspond to the overturned waves from the overhanging flanks on opposite sides of the salt. Figure 4 shows the model and rays in a tilted coordinate system with a tilting angle of 70°. Figures 3 and 4 illustrate that the waves that overturn in vertical Cartesian coordinates do not overturn in a tilted coordinate system with a well-chosen tilting direction.

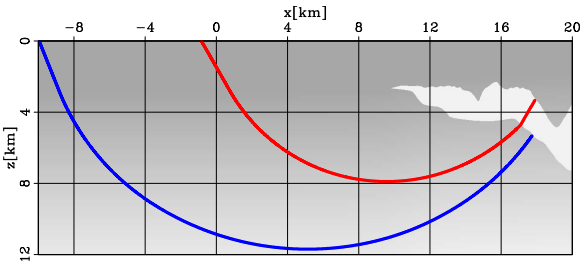

Figure 3: A velocity model revised from Sigsbee 2A. The sediment parts of the model are extended to allow the overturned waves from the overhanging salt flanks to be received at the surface. The rays represent the overturned waves from the overhanging salt flank.

PLANE-WAVE MIGRATION IN TILTED COORDINATES

We introduced the concepts of plane-wave migration and migration in tilted coordinates in previous sections. In this section, we discuss the combination of these two and provide a powerful method for migrating steeply dipping and overturned events. We first discuss why point-source migration in tilted coordinates would not be effective. Then we describe how to design tilted coordinates for each plane-wave source. Finally, we discuss how reciprocity improves plane-wave migration in tilted coordinates.

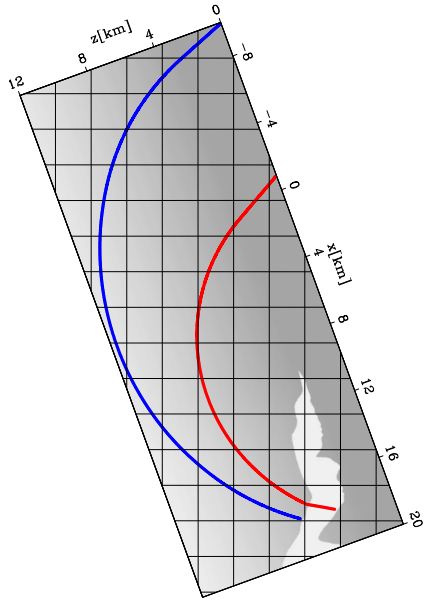

Figure 4: The velocity model and overturned waves in a tilted coordinate system. The overturned waves in vertical Cartesian coordinates do not overturn in the tilted coordinate system.

Waves from a point source propagate radially, and waves start from one spatial location and travel along all directions. Therefore, it is impossible for a tilted coordinate system to cover all the propagation directions of a point source. Figure 5a illustrates the waves from a point source in tilted coordinates. In Figure 5a the coordinates (x, z) are rotated counter-clockwise, where the high-angle energy can be well modeled on the right side, but the left-side energy (represented by dash-lines) cannot be modeled accurately, even for small-angle energy in vertical Cartesian coordinates. However, the propagation direction of a plane-wave source at different spatial locations is usually similar (Figure 5b). In plane-wave migration, we decompose the wavefield into plane-wave source gathers by slant-stacking, and each plane-wave source gather is characterized by a ray-parameter p_x. Given the velocity at the surface v_{z_0}, the propagation direction of the plane-wave source is defined by the vector (q_x, q_z), where $q_x = p_x v_{z_0}$ and $q_z = \sqrt{1 - q_x^2}$. Therefore, the ray parameter p_x defines the propagation direction of the plane-wave source at the surface. The take-off angle α of the plane-wave source can be calculated as follows:

$$\alpha = \arccos(q_x). \tag{15}$$

If we assume the velocity to be invariant at the surface, the propagation direction of the plane-wave source defined in equation 7 at the surface is the same for all spatial points. This is true for a marine dataset, and nearly true for a land dataset, if the velocity does not vary strongly at the surface. Therefore, a tilted coordinate system can cover most of the propagation directions of a plane-wave source from different spatial points, although the propagation direction of the plane-wave may change due to velocity heterogeneities.

Given a plane-wave source with a take-off angle of α, we use tilted coordinates (x', z'), with a tilting angle θ close to its take-off angle α. Usually, velocity increases with depth and the propagation direction of waves becomes increasingly horizontal, so in practice the tilting angle θ is a little larger than the take-off angle. Figure 6 shows three typical plane-wave sources and their tilted coordinate systems. Plane-wave sources with a small take-off angle mainly illuminate reflectors that are almost flat, so we extrapolate wavefields vertically. In contrast, plane-wave sources with a large take-off angle mainly illuminate steeply dipping reflectors, so we use a tilted coordinate system with a large tilting angle. Usually, these wavefields are difficult to extrapolate accurately by downward continuation migration, but in tilted coordinates their propagation direction is close to the extrapolation direction, so they can be imaged correctly. Waves overturning in vertical Cartesian coordinates do not overturn in a well-chosen tilted coordinate system. Therefore, in plane-wave migration in tilted coordinates, each plane-wave source has its own tilted coordinate system in which the extrapolation direction is close to the propagation direction, and steep reflectors and overturned waves can be imaged correctly.

Usually, in streamer acquisition we only record one-sided offset data at the surface. But we can obtain the data for the other side by reciprocity. Merging the original data and the data obtained by reciprocity, we obtain a dataset that would be recorded if

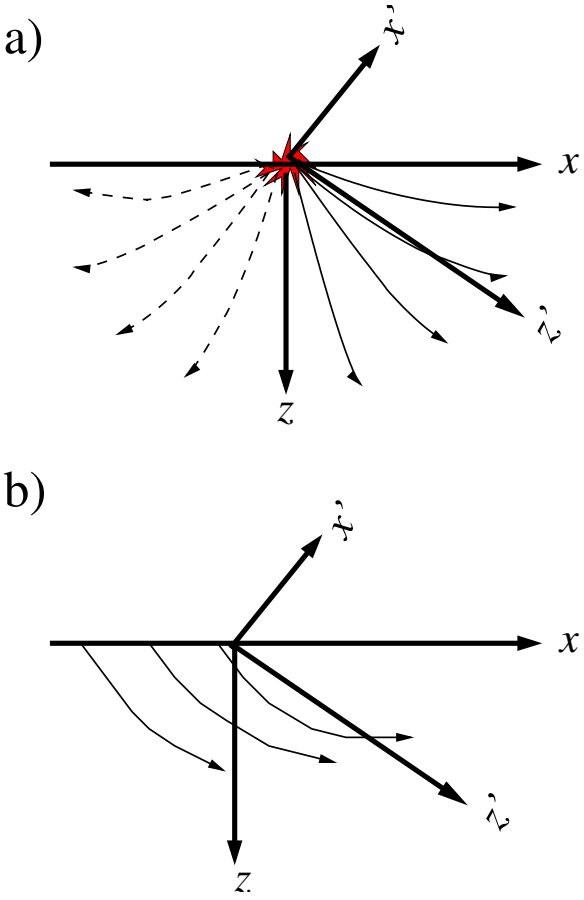

Figure 5: Point source (a) and plane-wave sources (b) in tilted coordinates. Waves from a point source propagate radially, and the waves represented by the dash line rays in panel (a) can not be caught when we rotate the coordinates counter-clockwise. In contrast, the propagation directions of the plane-wave source are similar in different spatial points, so most of them can be extrapolated accurately in a tilted coordinate system.

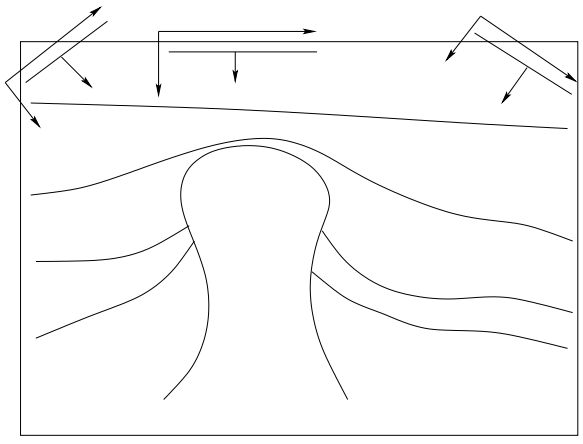

Figure 6: Plane-wave sources and their tilted coordinates. The tilting direction for the coordinates corresponding to the plane-wave source depends on its take-off angle. There are three typical plane-wave sources, and they have 0, negative and positive ray parameters, respectively. For $p = 0$, we use conventional Cartesian coordinates. For $p > 0$, we rotate coordinates counter-clockwise and for $p < 0$, we rotate coordinates clockwise.

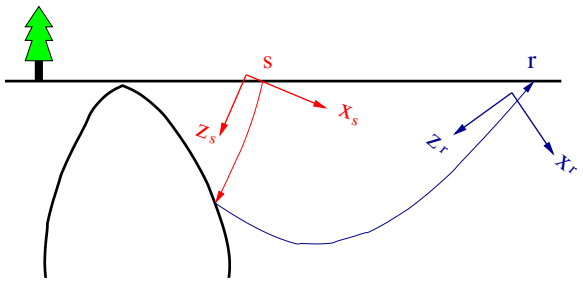

Figure 7: Reciprocity improves plane-wave migration in tilted coordinates. The source location is at s, and the receiver location is at r. For this event, the source ray does not overturn, but the receiver ray does. If we run plane-wave migration in tilted coordinates on the original one-sided offset data, we will use the coordinates (x_s, z_s), whose direction is determined by the source ray direction at the surface. In this coordinate system, the source waves can be handled but the overturned receiver wave cannot. If we run the same migration on the other side offset data generated by reciprocity, we will use the coordinates (x_r, z_r) for wavefield extrapolation, whose direction is determined by the receiver ray direction at the surface. In this coordinate system, both the source and receiver waves can be handled.

we would have had a split-spread recording geometry. In plane-wave migration for a dataset with a split-spread geometry, the aperture of each plane-wave source is almost the same as one-sided offset dataset, and thus the computation cost is also almost the same. But a split-spread recording geometry improves the plane-wave gathers and the signal-to-noise ratio of the image (Liu et al., 2006).

Reciprocity yields other benefits for plane-wave migration in tilted coordinates. Figure 7 illustrates how reciprocity helps to image steep salt flanks when the source ray does not overturn but the receiver ray does. In Figure 7, the source location is s and receiver location is r. For the original data, we run plane-wave migration for this event using the coordinates (x_s, z_s), whose tilting angle is determined by the source ray direction at the surface. The source plane wave starts at the surface almost vertically, and the tilting angle of its corresponding coordinates (x_s, z_s) is small. As a consequence, the overturned receiver wave cannot be accurately modeled, and the event cannot be correctly imaged. Reciprocity exchanges the source and receiver locations. For the data obtained by reciprocity, we run plane-wave migration for this event using the coordinates (x_r, z_r), whose direction is determined by the receiver ray direction at the surface. In the coordinates (x_r, z_r), both source and receiver waves can be accurately modeled, and the overturned energy can be correctly imaged. When we run plane-wave migration in tilted coordinates for a split-spread dataset, we design the coordinates considering the direction of both the source and receiver waves at the surface.

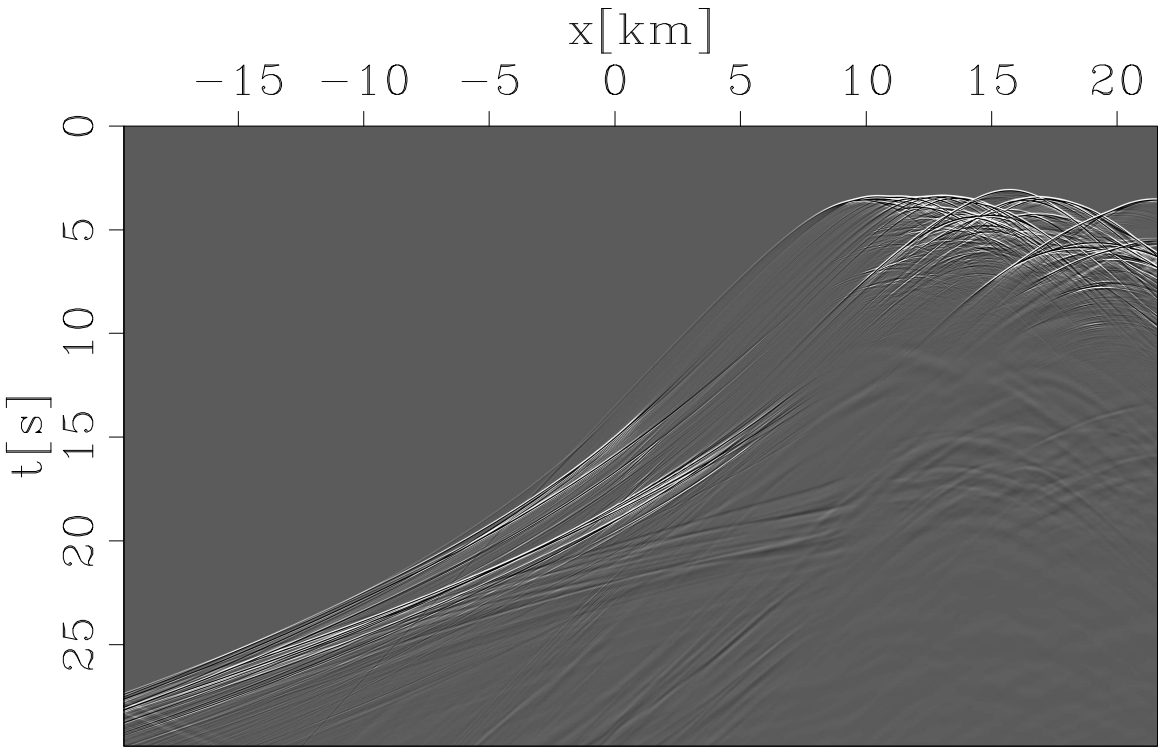

Figure 8: The exploding reflector dataset from the revised Sigsbee 2A model. The overturned energy is recorded from -20 to 5km at $t = 10$ to 25 s. The energy recorded earlier than 10 s is muted before migration to verify the imaging of overturned waves.

NUMERICAL EXAMPLES

An exploding-reflector dataset with overturned waves

Our first example is a synthetic dataset designed to test imaging of overturned waves (Sava, 2006). Figure 3 shows the model with typical overturned rays. The exploding reflector data are modeled from the boundary of the salt and recorded at the surface. The data are modeled using the time-domain two-way wave equation. Figure 8 shows the exploding reflector data received at the surface. The overturned events are recorded from $x = -20$ to 5 km at $t = 10$ to 25s.

To verify the extrapolation of overturned waves in tilted coordinates, we mute the non-overturned events that are received at the surface earlier than 10s. We migrate the dataset using a tilted coordinate system with a tilting angle of 70°, as shown in Figure 4. As demonstrated in the previous section, the waves illuminating the overhanging salt flanks do not overturn in the tilted coordinate system (Figure 4). For comparison, we also migrate the dataset using reverse-time migration. Figure 9 compares the images from these two methods. Figure 9a is the migrated image obtained by plane-wave migration in tilted coordinates, and Figure 9b is the image obtained by reverse-time migration. The image from reverse-time migration has lower frequency;

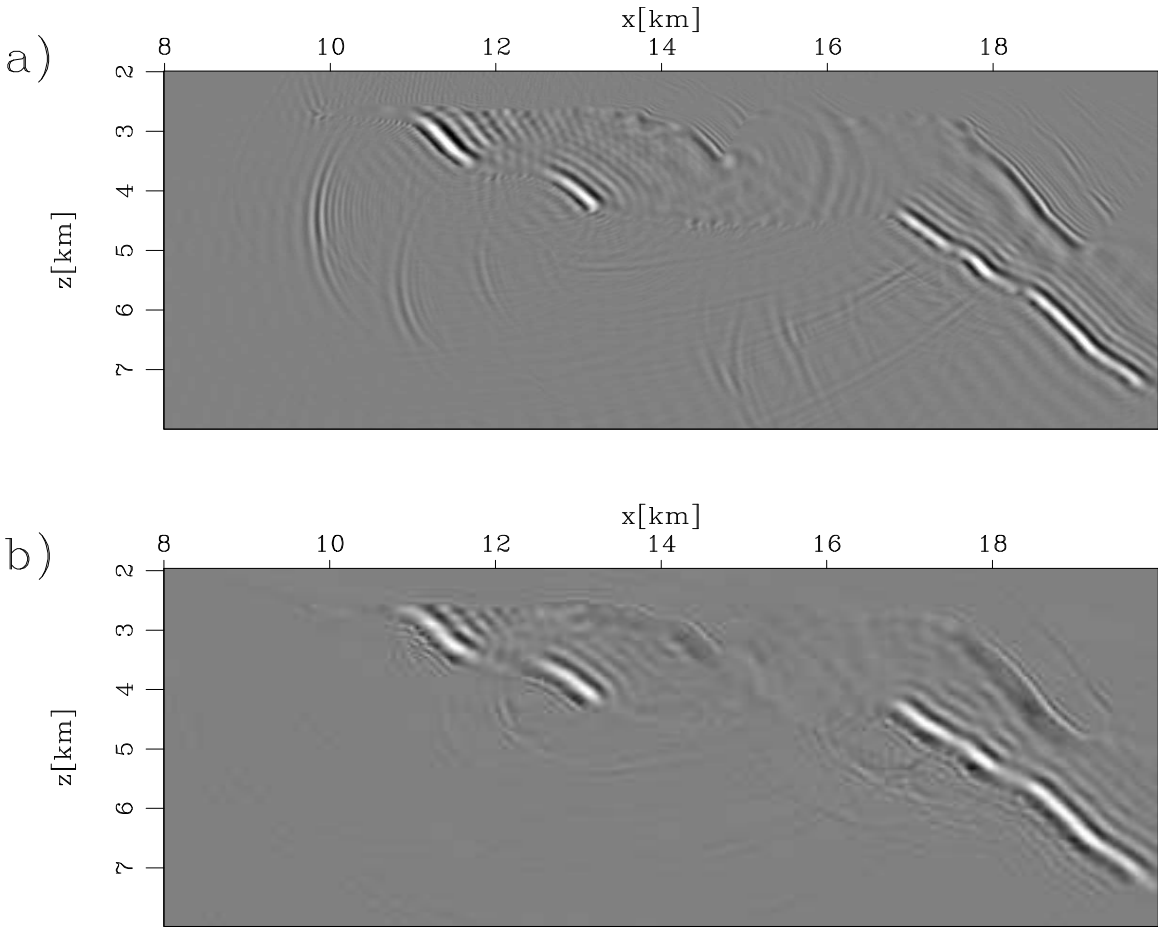

Figure 9: Migrated image of the overturned waves: migration in tilted coordinates (a) and reverse-time migration (b).

otherwise they are comparable. The comparison shows that most of the overturned energy is imaged by the migration in tilted coordinates, and all the overhanging salt flanks are imaged correctly.

Impulse responses

Our second example is a smooth sediment velocity field embedded with a salt body with steeply dipping flanks. Figure 10 is a comparison of the impulse responses of the two-way wave equation (Figure 10a), one-way wave-equation downward continuation (Figure 10b) and plane-wave migration in tilted coordinates (Figure 10c). From Figures 10a and b, we observe that the one-way wave equation mimics the two-way wave equation well for energy that propagates with small angles from the vertical direction, but its accuracy drops for energy that propagates almost horizontally. Energy that overturns is lost entirely. Comparing Figure 10c with Figure 10a, we notice that there are no reflections or multiples in Figure 10c. This is not surprising, since

the one-way wave-equation extrapolator is applied. But the wave front of the direct arrival matches that of the two-way wave equation very well, even at high angles and with overturned waves, despite being extrapolated with the one-way wave equation. The impulse-response comparison shows the potential to image the steeply dipping reflectors and overturned waves by plane-wave migration in tilted coordinates.

BP 2004 velocity benchmark dataset

The BP 2004 velocity benchmark dataset is designed to test velocity estimation. Figure 11 shows the velocity model of the dataset. One of the challenges for velocity analysis of this dataset is the delineation of the two salt bodies. The salt body on the left, modeled after a salt body in the Gulf of Mexico, is a complex, multi-valued salt body with a greatly rugose top. Some parts of its top, flanks and the sediment intrusion inside the salt are steeply dipping. It is difficult for downward continuation migration to image these features. The salt body on the right, modeled after a salt body in the western Africa, is deeply rooted, and its roots are very steep. Overturned and prismatic waves play a key role in imaging the two roots of the right salt body. Downward continuation loses the overturned energy and cannot connect these two roots. Even with the true velocity, it is challenging to image these complex salt bodies.

We run both plane-wave migrations in tilted coordinates and downward continuation migration for comparison. Two hundred plane-wave sources are generated in total, and the take-off angles at the surface range from -45° to 45°. No attempt is made to attenuate multiples, thus the images are contaminated by the multiples. The 80° finite-difference one-way extrapolator (Lee and Suh, 1985) is applied for both migrations.

Figure 12 shows the velocity model of the left salt body. Figure 13 and Figure 14 compare the images from the two migrations. Notice that remarks A, B, C, D, E, F, G and H in Figures 12, 13 and 14 are in exactly the same locations. Figures 13 and 14 are the images obtained by plane-wave migration in tilted coordinates and downward continuation migration, respectively. In both figures, the bottom of the big salt canyon is well imaged. But the steep flanks of the canyon at A and B, which are absent in Figure 14, are correctly imaged in Figure 13. This is also true for the small salt canyon at C. Although the salt canyon flank at D is imaged by downward continuation migration in Figure 14, it is not positioned correctly due to the limited accuracy of the operator compared to the model (Figure 12). The rugose top of the salt in Figure 13 is more continuous than that in Figure 14. The steep salt flanks in the multi-valued part at E, F and G and the sediment intrusion below the small salt canyon at H are greatly improved in Figure 13 by plane-wave migration in tilted coordinates, because they are illuminated by overturned or high-angle energy, which cannot be handled by downward continuation migration.

Figure 15 shows the velocity model of salt body on the right. Figure 16 and Figure

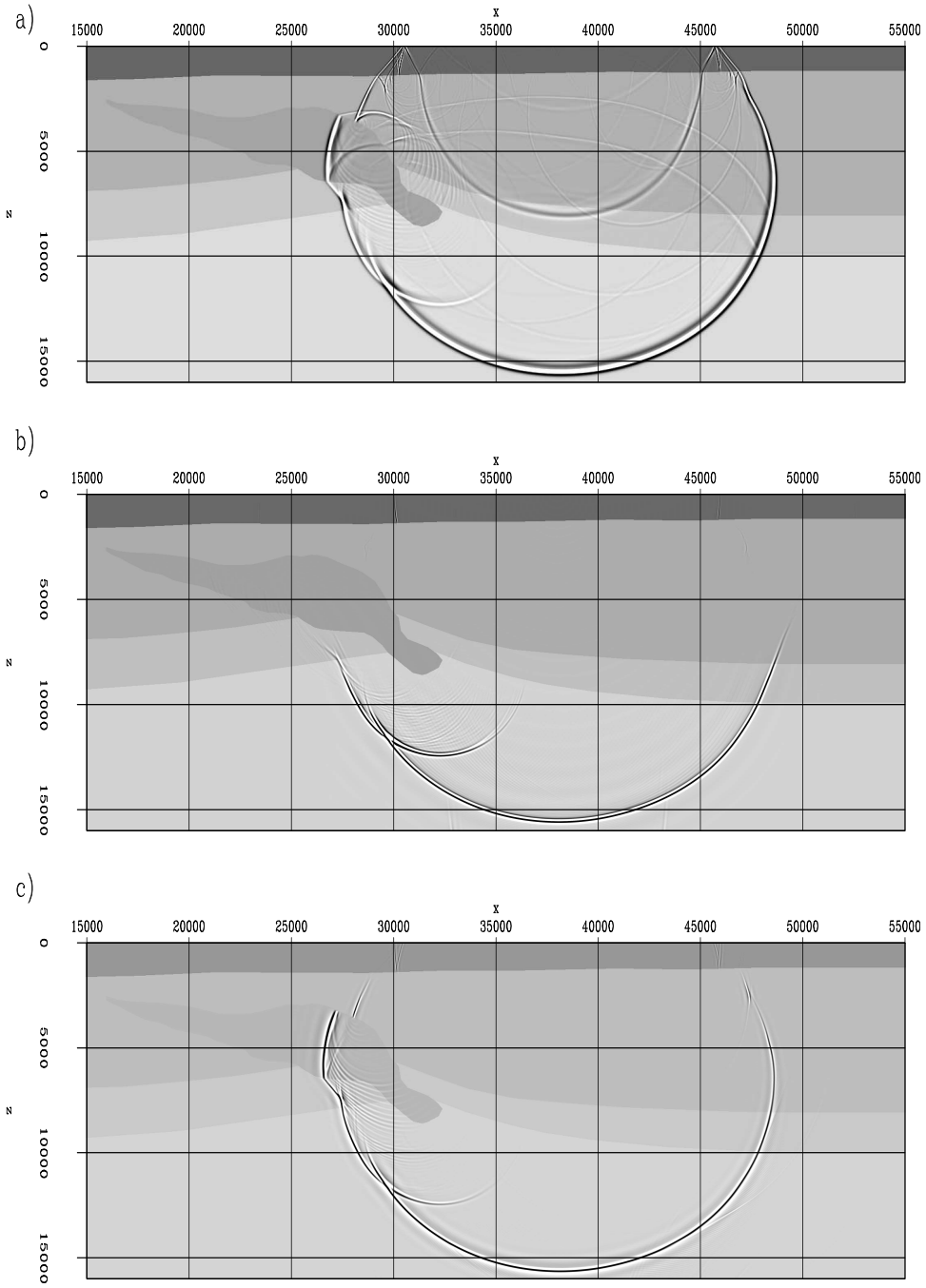

Figure 10: Impulse response comparison among (a) two-way wave equation, (b) one-way wave-equation downward continuation and (c) plane-wave migration in tilted coordinates.

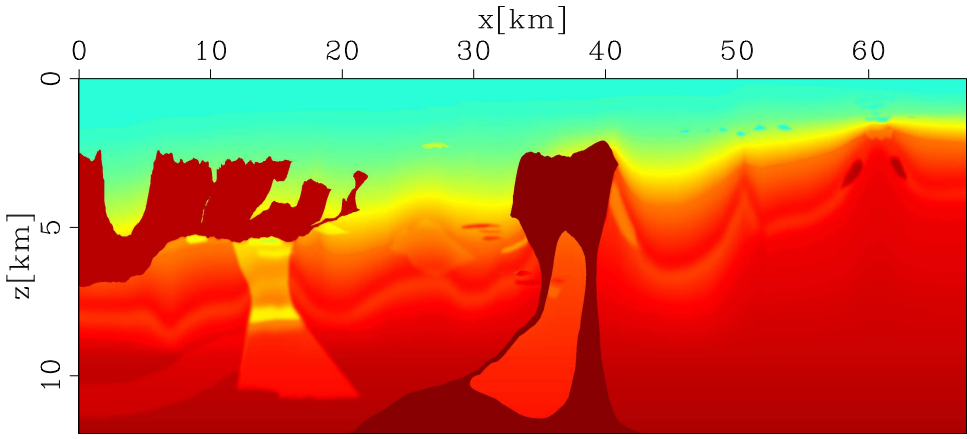

Figure 11: The velocity model of the BP velocity benchmark.

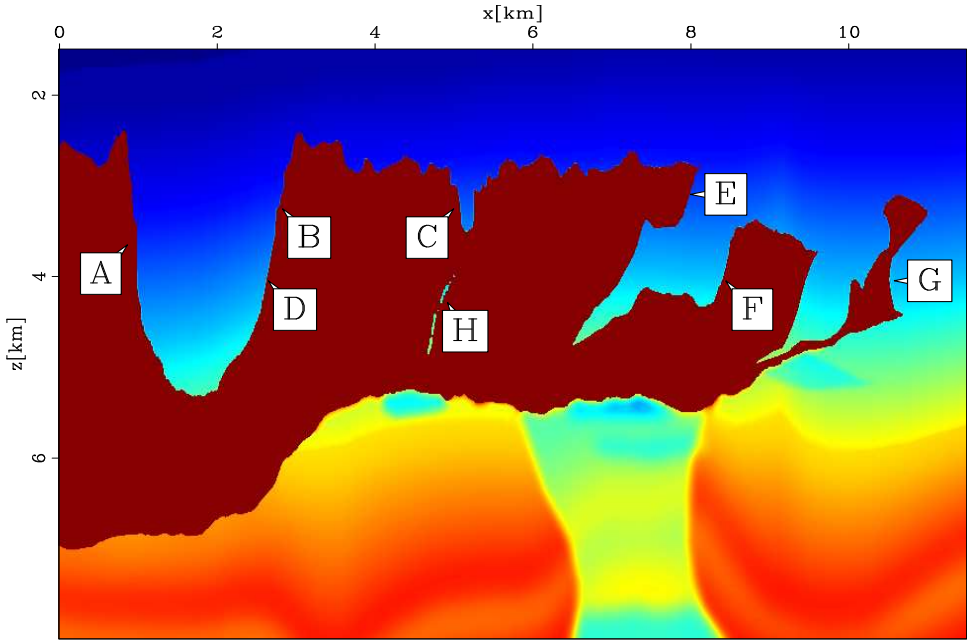

Figure 12: The velocity model of the left salt body.

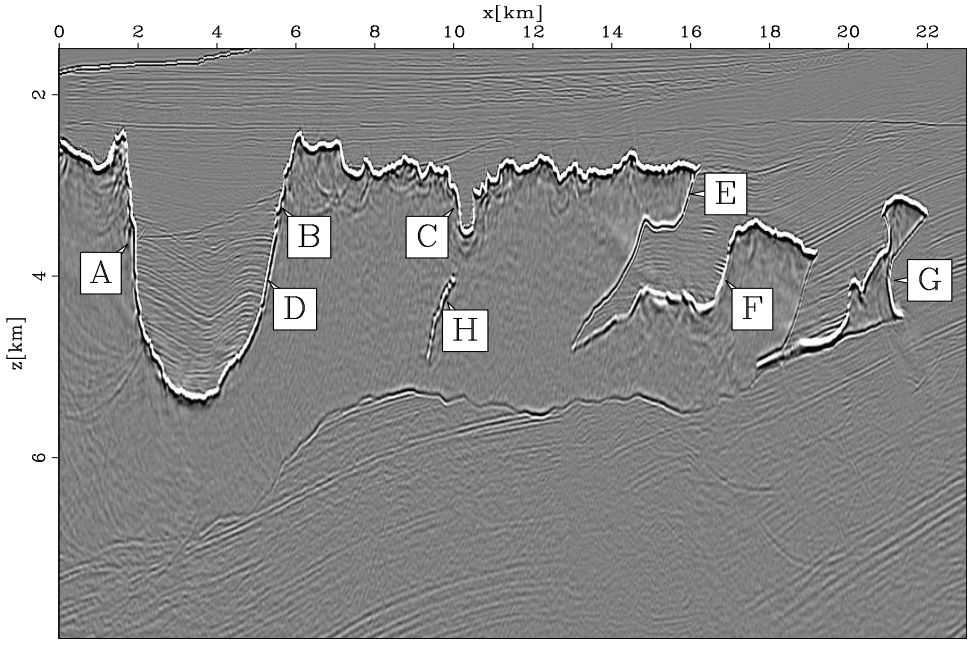

Figure 13: The images of the left salt body obtained by plane-wave migration in tilted coordinates.

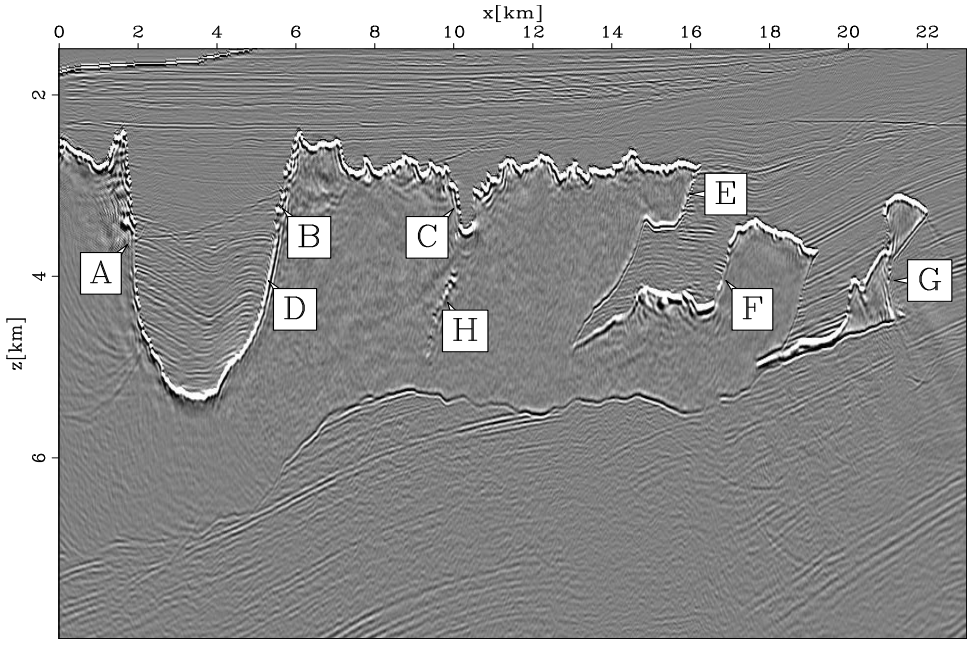

Figure 14: The images of the left salt body obtained by downward continuation migration.

17 compare the images from the two migrations. Notice that remarks A, B, C, D and E in Figures 15, 16 and 17 are in exactly the same locations. Figure 16 is obtained by plane-wave migration in tilted coordinates, and Figure 17 is obtained by downward continuation migration. The top of the salt and sediments inside the salt are well imaged in both figures. But the salt flanks at A, B and D that are illuminated by the overturned or high-angle energy in vertical Cartesian coordinates are absent in Figure 17. In contrast, this overturned energy is handled by plane-wave migration in tilted coordinates, producing a good image of the flanks of the salt roots. In Figure 17, we can see the steep flank at C, but it is not correctly positioned compared to Figure 16 because of the limited accuracy of the wavefield extrapolator. Note that the salt flank at E is absent in both images. This flank is illuminated mainly by prismatic waves which bounce off the salt root below E. The propagation direction of the prismatic waves varies greatly before and after the bounce at the salt boundary, and it is difficult to model them accurately in one coordinate system.

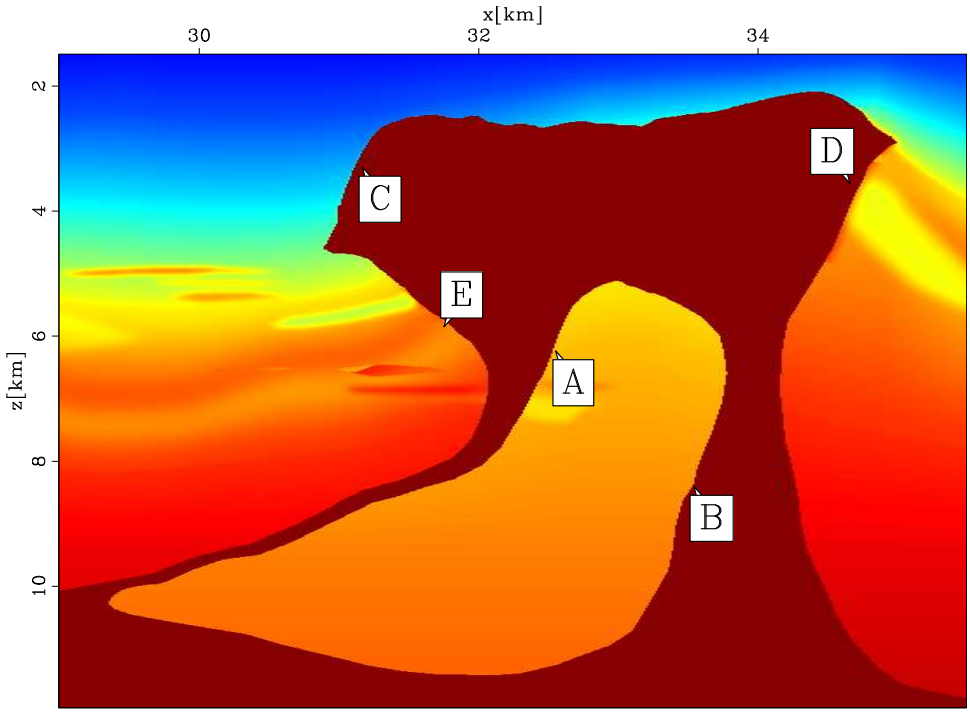

Figure 15: The velocity model of the right salt body.

Figures 13, 14, 16 and 17 show that plane-wave migration in tilted coordinates can handle overturned and high-angle energy and delineate complex salt bodies much better than downward continuation migration.

CONCLUSION

Plane-wave migration in tilted coordinates makes the extrapolation direction close to the actual propagation direction in the subsurface by assigning a well-chosen tilted

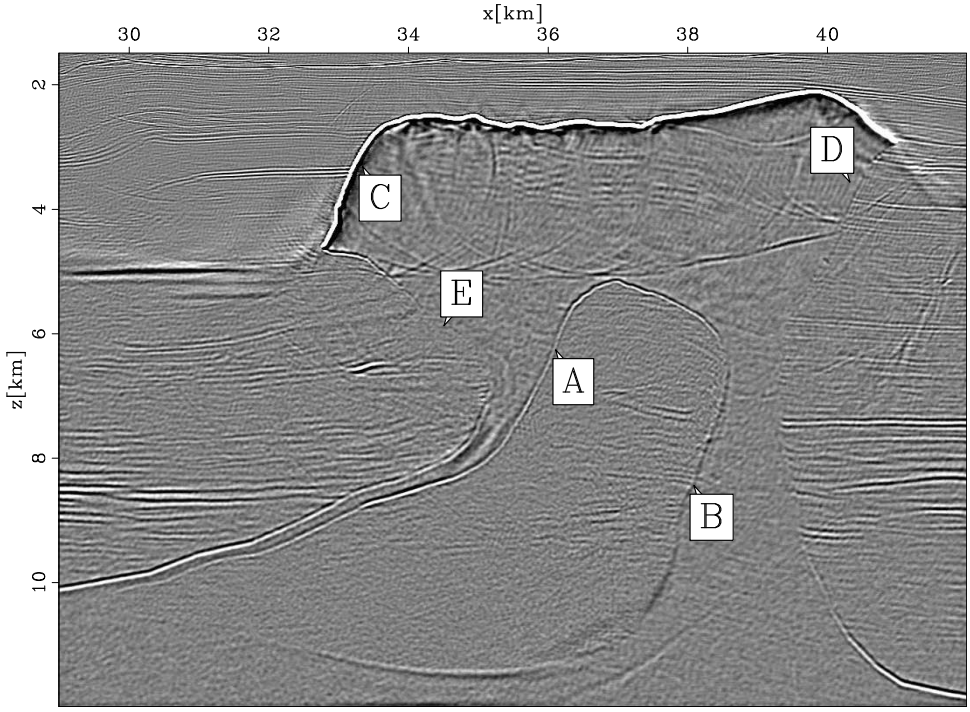

Figure 16: The images of the right salt body obtained by plane-wave migration in tilted coordinates.

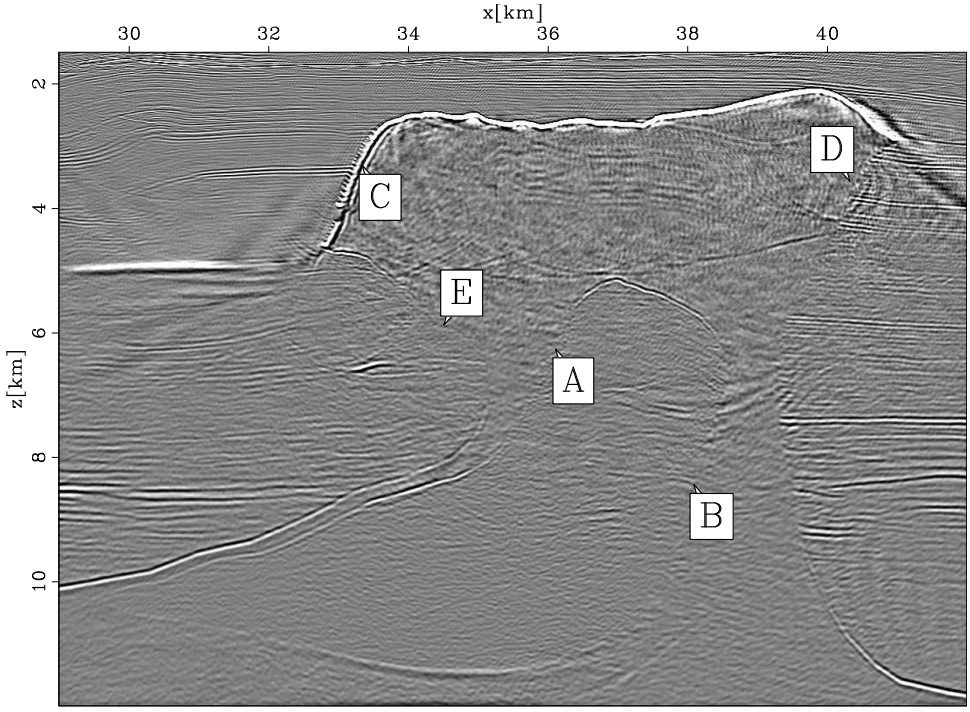

Figure 17: The images of the right salt body obtained by downward continuation migration.

coordinate system for each plane-wave source. One-way wave equations in tilted coordinates are exactly the same as those in vertical Cartesian coordinates, therefore we can still use the accurate one-way extrapolator methods developed for vertical Cartesian coordinates in last two decades to reduce the sensitivity to the coordinates. Plane-wave migration in tilted coordinates is much cheaper than reverse-time migration, but it can handle waves that illuminate steeply dipping reflectors and overhanging flanks, such as high-angle energy and overturned waves, which are challenging to image with conventional one-way downward continuation migration. Examples show that plane-wave migration in tilted coordinates is a good tool for delineation of complex salt bodies.

ACKNOWLEDGMENTS

We thank John Etgen of BP Upstream Technology Group for helpful discussion, Amerada Hess and BP for the synthetic datasets, and Paul Sava for the exploding reflector dataset.

REFERENCES

Baysal, E., D. D. Kosloff, and J. W. C. Sherwood, 1983, Reverse time migration: Geophysics, **48**, 1514–1524.

Biondi, B., 2002, Stable wide-angle Fourier finite-difference downward extrapolation of 3-D wavefields: Geophysics, **67**, 872–882.

Biondi, B. and G. Shan, 2002, Prestack imaging of overturned reflections by reverse time migration, *in* Expanded Abstracts, 1284–1287, Soc. of Expl. Geophys., 72^{nd} Ann. Internat. Mtg.

Claerbout, J. F., 1971, Toward a unified theory of reflector mapping: Geophysics, **36**, 467–481.

———, 1985, Imaging the Earth's interior: Blackwell Scientific Publications.

de Hoop, M. V., 1996, Generalization of the Bremmer coupling series: J. Math. Phys., 3246–3282.

Duquet, B., P. Lailly, and A. Ehinger, 2001, 3D plane wave migration of streamer data, *in* 71st Ann. Internat. Mtg, 1033–1036, Soc. of Expl. Geophys.

Etgen, J., 2002, Waves, beams and dimensions: an illuminating if incoherent view of the future of migration: Presented at the 72nd Ann. Internat. Mtg, Soc. of Expl. Geophys.

———, 2005, How many angles do we really need for delayed-shot migration?, *in* Expanded Abstracts, 1985–1988, Soc. of Expl. Geophys., 74^{th} Ann. Internat. Mtg.

Gazdag, J., 1978, Wave equation migration with the phase-shift method: Geophysics, **43**, 1342–1351.

Higginbotham, J. H., Y. Shin, and D. V. Sukup, 1985, Directional depth migration (short note): Geophysics, **50**, 1784–1796.

Huang, L. Y. and R. S. Wu, 1996, Prestack depth migration with acoustic screen propagators, *in* 66th Ann. Internat. Mtg, 415–418, Soc. of Expl. Geophys.

Lee, M. W. and S. Y. Suh, 1985, Optimization of one-way wave-equations (short note): Geophysics, **50**, 1634–1637.

Li, Z., 1991, Compensating finite-difference errors in 3-D migration and modeling: Geophysics, **56**, 1650–1660.

Liu, F., D. Hanson, N. Whitmore, R. Day, and R. Stolt, 2006, Toward a unified analysis for source plane-wave migration: Geophysics, **71**, S129–S139.

Liu, F., R. Stolt, D. Hanson, and R. Day, 2002, Plane wave source composition: An accurate phase encoding scheme for prestack migration, *in* 72nd Ann. Internat. Mtg, 1156–1159, Soc. of Expl. Geophys.

Nichols, D., 1994, Imaging in complex structures using band-limited green's function, *in* Ph.D. thesis, Stanford University.

Rietveld, W. E. A., 1995, Controlled illumination of prestack seismic migration, *in* Ph.D. thesis, Delft University of Technology.

Ristow, D. and T. Ruhl, 1994, Fourier finite-difference migration: Geophysics, **59**, 1882–1893.

Sava, P., 2006, Imaging overturning reflections by Riemannian wavefield extrapolation: Journal of Seismic Exploration, **15**, 209–223.

Sava, P. and S. Fomel, 2005, Riemannian wavefield extrapolation: Geophysics, **70**, T45–T56.

Shragge, J., 2006, Non-orthogonal Riemannian wavefield extrapolation, *in* Expanded Abstracts, 2236–2240, Soc. of Expl. Geophys., 75^{th} Ann. Internat. Mtg.

Whitmore, N. D., 1983, Iterative depth migration by backward time propagation, *in* 53rd Ann. Internat. Mtg, Session:S10.1, Soc. of Expl. Geophys.

———, 1995, An imaging hierarchy for common angle plane wave seismograms, *in* Ph.D. thesis, University of Tulsa.

Zhang, G., 1993, System of coupled equations for up-going and down-going waves: Acta Mathematicae Sinica, **16**, 251–263.

Zhang, J. and G. A. McMechan, 1997, Turning wave migration by horizontal extrapolation: Geophysics, **62**, 291–297.

Zhang, Y., J. Sun, C. Notfors, S. Gray, L. Chernis, and J. Young, 2005, Delayed-shot 3D depth migration: Geophysics, **70**, E21–E28.